26.457 Notes on Hamiltonians and Conservative Systems

Following on from the Newtonian description of dynamics in terms of force = mass x acceleration and the relationship between energy and work, Lagrange and Hamilton successively refined the description of dynamics into a coordinate-free description which holds equally for Cartesian, polar and other generalized coordinate systems.

The classical Hamiltonian and Lagrangian dynamical equations, are both expressed as differential equations defining generalized coordinates as a function of increasing time. Generally we think of the q_i as position coordinates and the p_i as momenta, so in effect $p_i = m\,\dot{q}_i$.

The Lagrangian $\mathcal{L} = T - V$ where T = kinetic & V = potential energy. It is expressed as a second order differential equation in terms of the position coordinates.

$$\frac{d}{dt}\left(\frac{\partial \mathcal{L}}{\partial \dot{q}_i}\right) - \frac{\partial \mathcal{L}}{\partial q_i} = 0 \quad i = 1, \ldots, N \qquad [2.1]$$

This coincides with the idea that changes in the kinetic energy are exactly compensated for by changes in the potential energy. Note that specifying the initial conditions in a dynamical problem requires determining both the positions and velocities i.e. q_i and $\dot{q}_i$.

e.g. Simple harmonic motion $\ddot{x} = -x \quad m = k = 1 \qquad T = \frac{1}{2}(\dot{x})^2 \quad V = -\int F.\,dx = \int x\,dx = \frac{1}{2}(x)^2$

$$\mathcal{L} = \frac{1}{2}(\dot{x})^2 - \frac{1}{2}(x)^2 \text{ so} \qquad \frac{d}{dt}\left(\frac{\partial \mathcal{L}}{\partial \dot{q}_i}\right) - \frac{\partial \mathcal{L}}{\partial q_i} = \frac{d}{dt}(\dot{x}) - (-x) = \ddot{x} + x = 0$$

Hamilton refined this description by converting the second-order equations in q_i into first-order differential equations in positions q_i and momenta p_i (for m = 1, $p_i = \dot{q}_i$). This is always possible for any order of differential equation since we are just naming successive derivatives using new names. This is very useful for the topological approach to conservative and non-conservative dynamics since it enables us to describe <u>any</u> dynamical system as a first-order one by a change of variables. A first-order system can then be directly modelled as a vector field in the space of dynamical variables - *phase space.*

The Hamiltonian $\mathcal{H} = T + V$. gives the total conserved energy of the system. The Hamiltonian formulation has proven universally useful spanning areas from classical dynamics to the Schrödinger equation of the wave function in quantum mechanics :

Because we are now dealing with T + V , we can take twice the kinetic energy and subtract $\mathcal{L}$:

$$\mathcal{H} = \sum_i p_i \dot{q}_i - \mathcal{L}$$

The Hamiltonian system now satisfies first-order equations $\frac{\partial \mathcal{H}}{\partial p_i} = \dot{q}_i \qquad \frac{\partial \mathcal{H}}{\partial q_i} = -\dot{p}_i$ [2.2]

e.g. Simple harmonic motion $\ddot{x} = -x \quad m = k = 1$ as above. $\mathcal{H} = \frac{1}{2}(\dot{x})^2 + \frac{1}{2}(x)^2$

Let $y = \dot{x}$ then we have $y = \dot{x}$, $\ddot{x} = (\dot{x}) = \dot{y} = -x$, just the form of equations 2.2.

e.g. Henon-Heiles system. $\mathcal{H} = \underbrace{\frac{1}{2}(\dot{x})^2 + \frac{1}{2}(\dot{y})^2}_{\text{K.E. of 2-oscillators}} + \underbrace{\frac{1}{2}(x)^2 + \frac{1}{2}(y)^2}_{\text{P.E. of 2-oscillators}} + \underbrace{x^2 y - \frac{1}{3}(y)^3}_{\text{Energy linkage}}$

so $\frac{\partial \mathcal{H}}{\partial p_1} = \frac{\partial \mathcal{H}}{\partial \dot{x}} = \dot{x} = q_1$ trivially confirming the change of variables, similarly for y.

More importantly $-\ddot{x} = -\dot{p}_1 = \frac{\partial \mathcal{H}}{\partial q_1} = \frac{\partial \mathcal{H}}{\partial x} = x + 2xy$, and $-\ddot{y} = -\dot{p}_2 = \frac{\partial \mathcal{H}}{\partial q_2} = \frac{\partial \mathcal{H}}{\partial y} = y + x^2 - y^2$

or $\ddot{x} = -x - 2xy, \quad \ddot{y} = -y - x^2 + y^2.$

The program performs simple numerical integration by picking a small value d and evaluating

$$\ddot{x}_{n+1} = -\tilde{x}_n - 2x_n y_n, \quad \ddot{y}_{n+1} = -\tilde{y}_n - x_n^2 + y_n^2$$

then $\dot{x}_{n+1} = \dot{x}_n + d\ddot{x}_{n+1}, \quad \dot{y}_{n+1} = \dot{y}_n + d\ddot{y}_{n+1}$

and finally $x_{n+1} = x_n + d\dot{x}_{n+1}, \quad y_{n+1} = y_n + d\dot{y}_{n+1}.$

The four variables x, y, $\dot{x}$ and $\dot{y}$ determine the dynamics and hence the energy. The program examines the dynamics in the $(y,\dot{y})$-plane and either looks at orbits of the second oscillator or the phase portrait gained by plotting a dot in this plane at each successive stroboscopic instant the x-oscillator is at x = 0. This is very similar to taking a Poincare map of the dynamical system. To get the starting condition of the remaining variable $\dot{x}$, we use the Hamiltonian expression for the total energy, :

$\dot{x} = \sqrt{2e - \dot{y}^2 - y^2 + \frac{2}{3}y^3}$ noting that the x^2 and 2xy terms are zero since x = 0.

eg. Simple - pendulum.

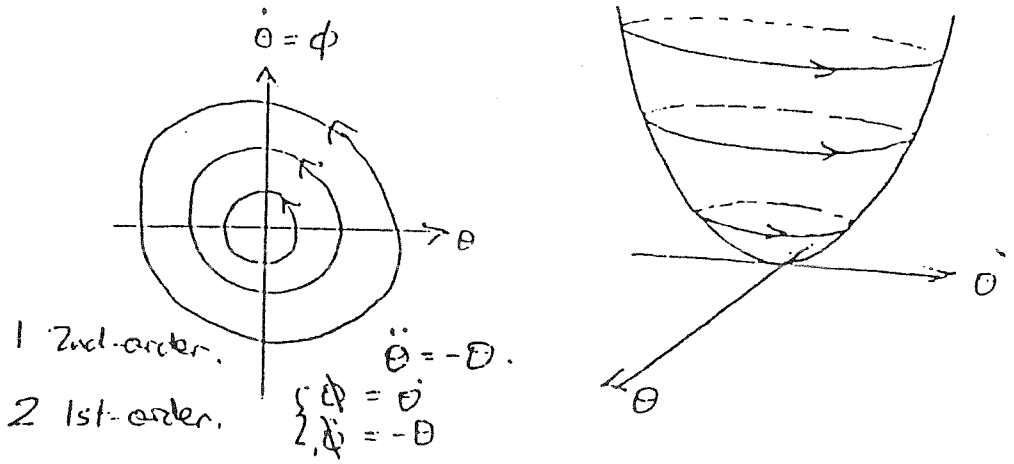

$\ddot{\theta} = -\sin\theta$.

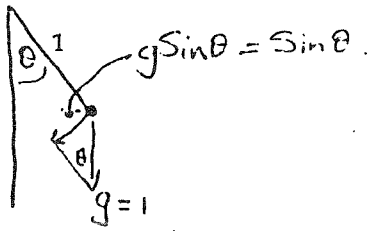

$V = \int \underset{\sim}{F} \cdot d\underset{\sim}{x} = \int \sin\theta \, d\theta$

$\underset{\sim}{x} = 1.0 \quad \underset{\sim}{F} = \sin\theta$.

Hence To consider Total energy.

$$\tfrac{1}{2}\dot{\theta}^2 - \cos\theta = C$$

Thus for any C plot $\dot{\theta} = \pm\sqrt{2C + 2\cos\theta}$.

We get.

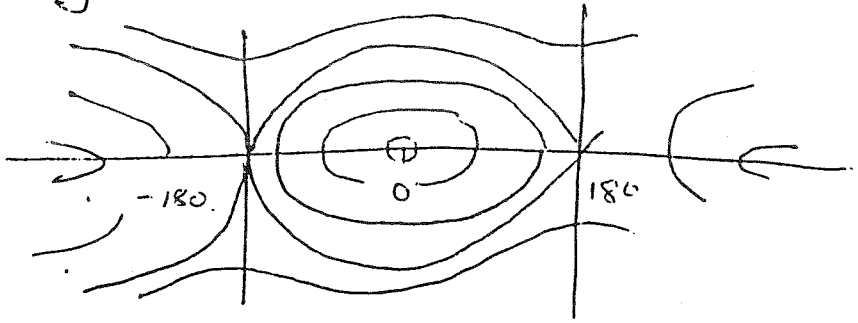

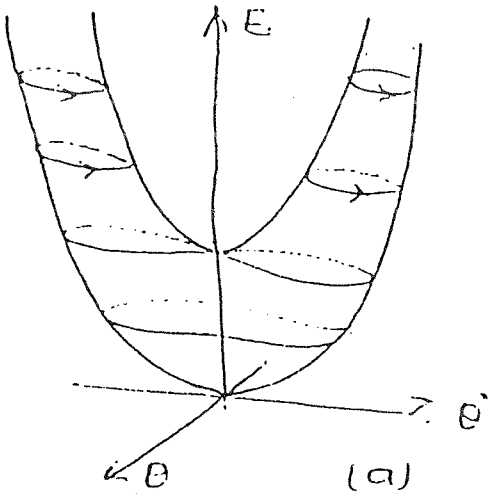

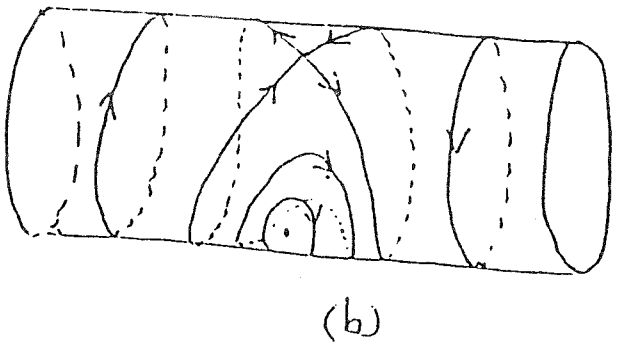

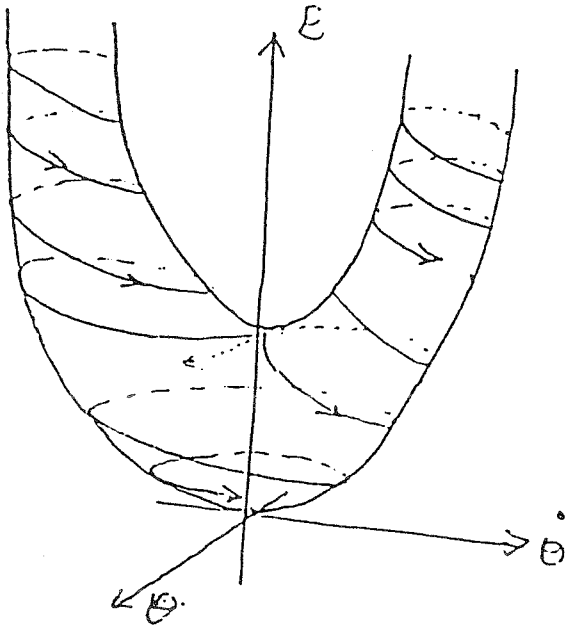

Fig 1.3 Dissipative field.

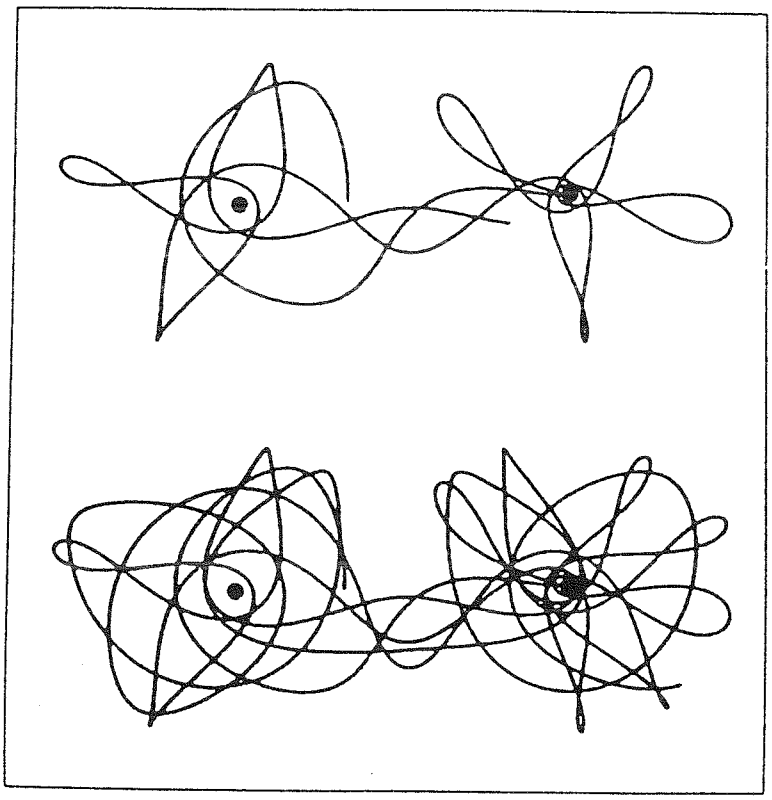

Figure 23 The complexities of three-body motion: here a dust particle orbits two fixed planets of equal mass.

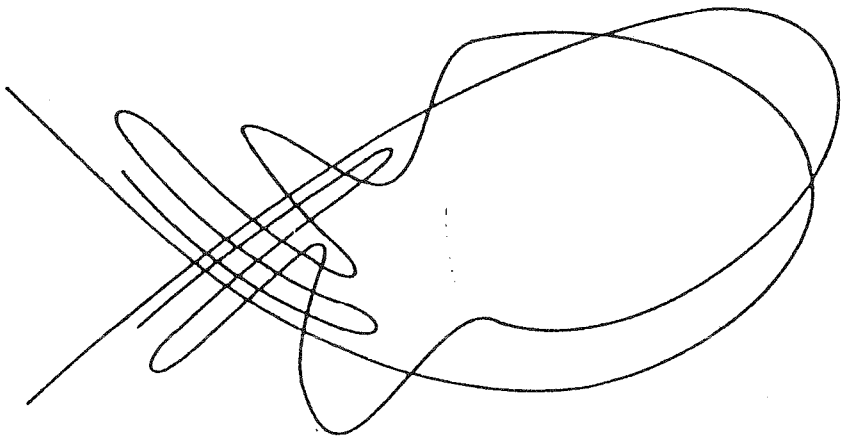

Figure 26 Footprints of chaos in the sands of time. . . Homoclinic tangles in the three-body problem. Poincaré was horrified.

A classical deterministic system following the principles of the Laplacian universe can be described by specifying its equations of evolution and the initial conditions. Often the equations of evolution take the form of differential equations. The classical Hamiltonian and Lagrangian dynamical equations, for example, are both expressed as differential equations defining generalized coordinates as a function of increasing time, where $\mathcal{L} = T - V$ and in the case of a potential, $\mathcal{H} = T + V$, giving the total (T kinetic & V potential) energy :

$$\frac{d}{dt}\left(\frac{\partial \mathcal{L}}{\partial \dot{q}_i}\right) - \frac{\partial \mathcal{L}}{\partial q_i} = 0 \quad i = 1, \ldots, N \qquad [2.1]$$

$$\dot{q}_i = \frac{\partial \mathcal{H}}{\partial p_i} \qquad \dot{p}_i = -\frac{\partial \mathcal{H}}{\partial q_i}$$

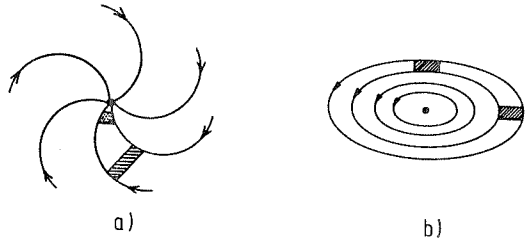

Fig. 125: a) In dissipative systems trajectories are attraced to fixed point, and volume shrinks, b) In conservative systems the points rotate around an elliptic fixed point, volume is conserved.

We now present some motivation for the study of conservative systems and then give an overview over the rest of this chapter.

For some time, attention has shifted from the calculation of individual orbits to consideration of the qualitative properties of families of orbits, as shown in Fig. 126. Today, we are mainly interested in the long-time behavior of conservative systems. There are several reasons for this:

a) We should, for example, be able to answer the question whether the solar systems and the galaxy are stable under mutual perturbations of their constituents, or whether they will eventually collapse or disperse to infinity. The long-time limit involved here is of the order of the age of the universe. But "long" times are much shorter in the storage rings used for high energy physics or in fusion experiments, where the particles make many revolutions in fractions of a second. In such systems irregular or chaotic motion is to be avoided at all costs, and this is only possible if the long-time behavior of these (conservative) systems is known.

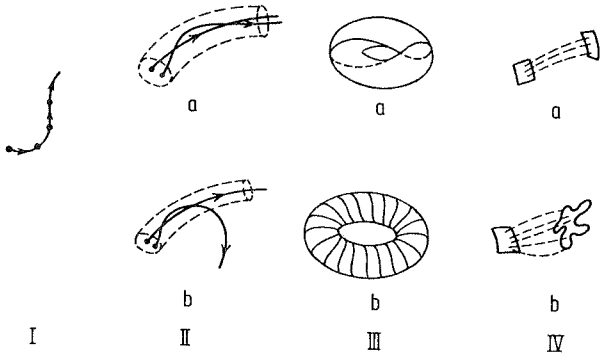

Fig. 126: Problems of increasing globality in classical mechanics. I. Step by step integration of the equations of motion. II. a) Local stability; b) local instability. III. Topological nature of complete trajectories: a) periodic motion on a torus; b) motion on a torus with irrational frequency ratios. IV. Types of flow in phase space: a) non mixing; b) mixing. (After Balescu, 1975.)

b) another point concerns the foundations of statistical mechanics, where no attempt is made to follow the detailed motion of all constituents of a complicated manybody problem. Instead, the ergodic hypothesis is made, i.e. one assumes that in the course of time the system explores the entire region of phase space allowed (the energy surface) and eventually covers this region uniformly. Time averages can then be replaced by simpler phase-space averages. But is the ergodic hypothesis correct? To answer this question, the long-time behavior of Hamiltonian systems with N degrees of freedom in the limit $N \to \infty$ (and N/volume = constant) must be known.

In the first part of this section, we consider the classical mechanis of simple Hamiltonian systems with a few degress of freedom and show that in most cases their motion in phase space is extremely complicated and neither regular nor simply ergodic. In other words, it will be shown that the regular motion treated in most textbooks on classical mechanics is an exception and rather uncommon.

In the second part, we discuss some simple model systems which behave ergodically although they have only a few degrees of freedom. Finally, a classification scheme for chaotic behavior in conservative systems is described.

7.1 Coexistence of Regular and Irregular Motion

In the following, we investigate the stability of the trajectories of a nonintegrable Hamiltonian system in the long-time limit. For this purpose, we start from an integrable Hamiltonian and consider the effect of a small nonintegrable perturbation.

Integrable Systems

A Hamiltonian $H_0'(\vec{p}, \vec{q})$ is called integrable if one can find a canonical transformation $S(\vec{q}, \vec{J})$ to new variables $\vec{\theta}$, $\vec{J}$:

$$\vec{q}, \vec{p} = \frac{\partial S(\vec{q}, \vec{J})}{\partial \vec{q}} \leftrightarrow \vec{J}, \vec{\theta} = \frac{\partial S(\vec{q}, \vec{J})}{\partial \vec{J}} \tag{7.3}$$

such that in the new coordinates the Hamiltonian depends only on the new momenta $\vec{J}$, *i.e.*, $S(\vec{q}, \vec{J})$ is a solution of the *Hamilton-Jacobi equation* (see, e.g., Arnold, 1978):

$$H_0'\left[\vec{q}, \frac{\partial S(\vec{q}, \vec{J})}{\partial \vec{q}}\right] = H_0(\vec{J}) \tag{7.4}$$

and the equations of motion in the action-angle variables $\vec{J}$ and $\vec{\theta}$

$$\dot{\vec{J}} = -\frac{\partial H_0}{\partial \vec{\theta}} = 0 \tag{7.5}$$

$$\dot{\vec{\theta}} = \frac{\partial H_0}{\partial \vec{J}} = \vec{\omega}(\vec{J})$$

can easily be integrated to

$$\vec{J} = \text{const.}$$
$$\vec{\theta} = \vec{\omega} \cdot t + \vec{\delta}\,. \tag{7.7}$$

One of the simplest examples for an integrable system is a harmonic oscillator that has the Hamiltonian

$$H_0' = \frac{1}{2}(p^2 + \omega^2 q^2)\,. \tag{7.8}$$

The Hamilton-Jacobi equation (7.4) then becomes

$$\frac{1}{2}\left[\left(\frac{\partial S}{\partial q}\right)^2 + \omega^2 q^2\right] = H_0(J) \tag{7.9}$$

$$\rightarrow \frac{\partial S}{\partial q} = \sqrt{2H_0 - \omega^2 q^2} \tag{7.10}$$

and J is determined by

$$J = \frac{1}{2\pi}\oint \frac{\partial S}{\partial q}\,\mathrm{d}q = \frac{H_0(J)}{\omega} \tag{7.11}$$

$$\rightarrow H_0(J) = J\omega \tag{7.12}$$

where the integral has been taken over one cycle of q.

The equations of motion in the action-angle variables are

$$\dot{J} = \frac{\partial H_0}{\partial \theta} = 0 \rightarrow J = \text{const} \tag{7.13a}$$

$$\dot{\theta} = \frac{\partial H_0}{\partial J} = \omega \rightarrow \theta = \omega t + \delta\,. \tag{7.13b}$$

The motion in the variables p and q is obtained from

$$\theta = \frac{\partial S}{\partial J} = \frac{\partial}{\partial J}\int \mathrm{d}q\,\sqrt{2H_0 - \omega^2 q^2} = \arccos\left(q\sqrt{\frac{\omega}{2J}}\right) \tag{7.14}$$

$$\rightarrow q = \sqrt{\frac{2J}{\omega}}\cos\theta \tag{7.15}$$

and

$$p = \frac{\partial S}{\partial q} = -\sqrt{2J\omega}\,\sin\theta\,. \tag{7.16}$$

The corresponding trajectory in phase space is an ellipse that becomes a circle with polar coordinates $\sqrt{J}$ and θ after proper rescaling. Comparing eqns. (7.7) and (7.13) one sees that the equations of motion (in action-angle variables) of any integrable system with n degrees of freedom are practically the same as those of a set of n uncoupled harmonic oscillators. The only difference is that in a general integrable system the frequencies ω_i are still functions of the actions J_i whereas they are independent of J_i for harmonic oscillators. The existence of n integrals of the motion $(J_1 \ldots J_n)$ confines the trajectory in the 2 n-dimensional phase space $(q_1 \ldots q_n, p_1 \ldots p_n)$ of an integrable system to an n-dimensional manifold which has – in analogy to a circle for a harmonic oscillator with $n = 1$ and a torus for two harmonic oscillators with $n = 2$ – the topology of an n-torus.

In the following, we will confine ourselves to $n = 2$, but most results can be extended to more degrees of freedom. Fig. 127 shows the motion of an integrable system with two degrees of freedom (i. e. with a 4-dimensional phase space) on a torus. Closed orbits occur only if

$$n\Delta\theta_2 = 2\pi \cdot m, \text{ i.e. } \frac{\omega_2}{\omega_1} = \frac{m}{n} = \text{rational}\,;\ m, n = 1, 2, 3 \ldots . \tag{7.17}$$

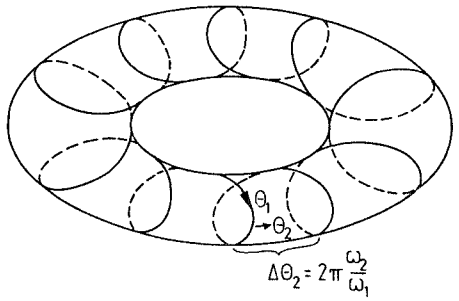

Fig. 127: Torus in phase space.

For irrational frequency ratios, the orbit never repeats itself but approaches every point on the two-dimensional manifold infinitesimally close in the course of time. In other words, the motion is ergodic on the torus. (Note that the dimension 2 of the torus is different from the dimension 3 of the manifold defined by $H(\vec{p}, \vec{q}) = E = \text{const.}$)

Perturbation Theory and Vanishing Denominators

Let us now add to H_0 a perturbation εH_1 and see how it effects the previously regular motion; that is, we consider the Hamiltonian

$$H(\vec{J}, \vec{\theta}) = H_0(\vec{J}) + \varepsilon H_1(\vec{J}, \vec{\theta}) \tag{7.18}$$

(where we expressed H_1 in the action-angle variables $\vec{J} = (J_1, J_2)$, $\vec{\theta} = (\theta_1, \theta_2)$ of the unperturbed system), and we try to solve the Hamilton-Jacobi equation

$$H\left[\frac{\partial S}{\partial \vec{\theta}}, \vec{\theta}\right] = H_{00}(\vec{J}') . \tag{7.19}$$

Writing the generating function S as

$$S(\vec{J}', \vec{\theta}) = \vec{\theta} \cdot \vec{J}' + \varepsilon S_1(\vec{J}', \vec{\theta}) \tag{7.20}$$

and expanding H to order ε, we obtain

$$H_0(\vec{J}') + \varepsilon \frac{\partial H_0}{\partial \vec{J}} \cdot \frac{\partial S_1(\vec{J}', \vec{\theta})}{\partial \vec{\theta}} + \varepsilon H_1(\vec{J}', \vec{\theta}) + O(\varepsilon^2) = H_{00}(\vec{J}') \tag{7.21}$$

S_1 is determined by requiring that the left-hand side in (7.21) is independent of $\vec{\theta}$, i.e.

$$\vec{\omega} \cdot \frac{\partial S_1(\vec{J}', \vec{\theta})}{\partial \vec{\theta}} = -H_1(\vec{J}', \vec{\theta}) \tag{7.22}$$

where $\vec{\omega} = \partial H_0 / \partial \vec{J}'$ are the frequencies of the unperturbed system. Eq. (7.21) can be solved by expanding S_1 and H_1 (both being periodic in the components of $\vec{\theta}$) into Fourier series:

$$S_1(\vec{J}', \vec{\theta}) = \sum_{\vec{K} \neq 0} S_{1,\vec{K}}(\vec{J}') e^{i\vec{K} \cdot \vec{\theta}} \tag{7.23a}$$

$$H_1(\vec{J}', \vec{\theta}) = \sum_{\vec{K} \neq 0} H_{1,K}(\vec{J}') e^{i\vec{K} \cdot \vec{\theta}} \tag{7.23b}$$

with $\vec{K} = 2\pi(n_1, n_2)$; n_1, n_2 integers.

Using both expressions in (7.22) and comparing equal Fourier components finally yields

$$S(\vec{J}', \vec{\theta}) = \vec{\theta} \cdot \vec{J}' + i\varepsilon \sum_{\vec{K} \neq 0} \frac{H_{1,K}(\vec{J}')}{\vec{K} \cdot \vec{\omega}(\vec{J}')} e^{i\vec{K} \cdot \vec{\theta}} . \tag{7.24}$$

Equation (7.24) shows that S diverges for

$$\omega_1 n_1 + \omega_2 n_2 = 0 , \text{ i.e. } \frac{\omega_1}{\omega_2} = -\frac{n_2}{n_1} = \text{rational} . \tag{7.25}$$

This is the famous problem of vanishing denominators. It shows that the system cannot be integrated by perturbation theory for rational frequency ratios because of strong resonances, and it seems that it can at most be integrated for irrational values of ω_1/ω_2 if the perturbation series in ε converges.

In the following we consider two problems:

- What happens if an integrable system with ω_1/ω_2 close to an *irrational* value is perturbed by εH_1?
- What happens under a perturbation εH_1 to the tori of a system for which ω_1/ω_2 has a *rational* value?

Stable Tori and KAM Theorem

The first question is answered by a celebrated theorem of Kolmogorov (1954), Arnold (1963), and Moser (1967), the so-called KAM theorem which we quote here for $n = 2$, without proof. (The theorem holds for an arbitrary number n of degrees of freedom and proofs can be found in the quoted references.) The theorem states that if, among other technical conditions, the Jacobian of the frequencies is nonzero, i.e.

$$\left| \frac{\partial \omega_i}{\partial J_j} \right| \neq 0 \tag{7.26}$$

then those tori, whose frequency ratio ω_2/ω_1 is sufficiently irrational such that

$$\left| \frac{\omega_1}{\omega_2} - \frac{m}{s} \right| > \frac{k(\varepsilon)}{s^{2.5}} \qquad (k(\varepsilon \to 0) \to 0) \tag{7.27}$$

holds (m and s are mutually prime integers), are stable under the perturbation εH_1 in the limit $\varepsilon \ll 1$.

It is important to note that the set of frequency ratios, for which (7.27) holds and for which the motion is therefore regular, even after the perturbation, has a nonzero

measure. This follows because the total length L of all intervals in $0 \le \omega_1/\omega_2 \le 1$, say, for which (7.27) *does not hold* can be estimated as

$$L < \sum_{s=1}^{\infty} \frac{k(\varepsilon)}{s^{2.5}} \cdot s = k(\varepsilon) \sum_{s=1}^{\infty} s^{-1.5} = \text{const.} \cdot k(\varepsilon) \to 0 \text{ for } \varepsilon \to 0 \,. \quad (7.28)$$

Here $k(\varepsilon)/s^{2.5}$ is the length of an interval around the rational m/s where (7.27) does not apply, and s is the number of m values with $m/s \le 1$ (see Fig. 128).

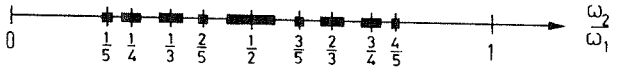

Fig. 128: Intervals of lengths $k(\varepsilon)/s^{2.5}$ contributing to L.

Eq. (7.28) means that the set of frequency ratios, for which (under a perturbation by εH_1) the original motion on the torus is only slightly disturbed into the motion of a deformed torus, has the finite measure $1 - \text{const.} \cdot k(\varepsilon)$. But, on the ω_1/ω_2 axis, this set has holes around every rational ω_1/ω_2.

For large enough ε the perturbation εH_1 destroys *all* tori. The last KAM torus which will be destroyed is the one for which the frequency ratio is the "worst irrational number" $\omega_1/\omega_2 = (\sqrt{5} - 1)/2$ (see Sect. 6.2). The destruction of this KAM torus shows some similarity to the Ruelle-Takens route to chaos in dissipative systems. It has indeed been found by Shenker and Kadanoff (1982) and McKay (1983) who studied the conservative version ($b = 1$) of the map (6.12) of the annulus onto itself that the decay of the last KAM trajectory shows scaling behavior and universal features.

Unstable Tori and Poincaré-Birkhoff Theorem

Let us now discuss the situation when ω_1/ω_2 is rational. We will show that in this case the original torus decomposes into smaller and smaller tori. Some of these newly created tori are again stable according to the KAM theorem. But, between the stable tori, the motion is completely irregular.

It is convenient to visualize what happens (to H_0 under a perturbation εH_1) in a Poincaré map that is, in general, defined by the intersection points of the orbit with a hyperplane in phase space. For the case in hand, we consider the intersections with the q_1, p_1 plane S shown in Fig. 129, which define an area-preserving two-dimensional map

$$\left.\begin{aligned} r_{i+1} &= r_i' \qquad r_i' = r\left(1 - i \cdot \frac{2\pi}{\omega_2}\right) \\ \theta_{i+1} &= \theta_i + 2\pi \frac{\omega_1}{\omega_2} \end{aligned}\right\} \quad (7.29)$$

since the point in phase space hits S after a period $2\pi/\omega_2$ during which θ changes by $2\pi\omega_1/\omega_2$.

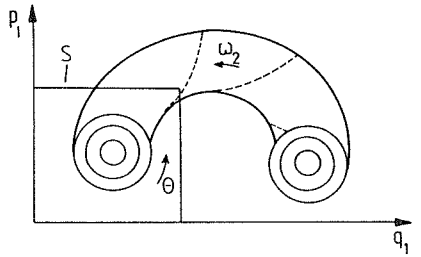

Fig. 129: Poincaré map of orbits on the torus in the plane (q_1, p_1).

The frequency ratio ω_1/ω_2 depends only on the radius r because

$$\left.\begin{aligned} \frac{\omega_1}{\omega_2} &= \frac{\dfrac{\partial H_0(J_1, J_2)}{\partial J_1}}{\dfrac{\partial H_0(J_1, J_2)}{\partial J_2}} = f(J_1, J_2) \\ H_0(J_1, J_2) &= E = J_2 = J_2(J_1) \\ J_1 &= \frac{1}{2\pi} \oint p_1 \, \mathrm{d}q_1 = \frac{r^2}{2} \end{aligned}\right\} \Rightarrow \frac{\omega_1}{\omega_2} = a(r) \quad (7.30)$$

(7.30) can therefore be written as

$$\left.\begin{aligned} r' &= r \\ \theta' &= \theta + 2\pi a(r) \end{aligned}\right\} \equiv T\begin{pmatrix} r \\ \theta \end{pmatrix}. \quad (7.31)$$

This is Moser's twist map (Moser, 1973).

We note that for a rational frequency ratio $r/s = a(r_0)$ every point on the circle r_0, θ_0 is a fixed point of T^s since

$$T^s \begin{pmatrix} r_0 \\ \theta_0 \end{pmatrix} = \begin{cases} r_0 \\ \theta_0 + 2\pi \dfrac{r}{s} \cdot s = \theta_0 + 2\pi r \,. \end{cases} \quad (7.32)$$

If we now perturb H_0 by εH_1, the twist map becomes

$$\left.\begin{aligned} r_{i+1} &= r_i + \varepsilon f(r_i, \theta_i) \\ \theta_{i+1} &= \theta_i + 2\pi a(r_i) + \varepsilon g(r_i, \theta_i) \end{aligned}\right\} = T_\varepsilon \begin{pmatrix} r_i \\ \theta_i \end{pmatrix} \quad (7.33)$$

where f and g depend on H_1. As a consequence of Liouville's theorem (which also holds for the Hamiltonian $H_0 + \varepsilon H_1$), the map T_ε is area-preserving.

What can we say now about the fixed points of T_ε? Consider two circles C_+ and C_- between which lies the circle C on which $a = r/s$. On C_+, $a > r/s$ and on C_-, $a < r/s$. T^s therefore maps C_+ anti-clockwise, C_- clockwise, and C not at all (see Fig. 130).

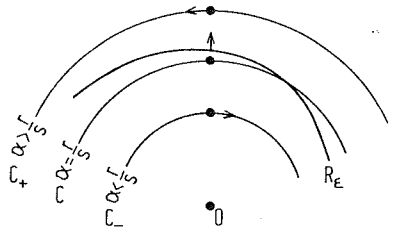

Fig. 130: Action of T^s and T^s_ε on C_+ and C_-.

Under the perturbed map T^s_ε these relative twists are preserved if ε is small enough. Thus, on any radius from 0 there must be one point whose angular coordinate is unchanged by T^s_ε. These radially mapped points make up a curve R_ε close to C.

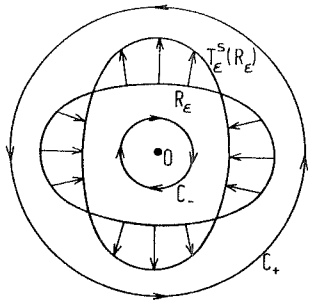

Fig. 131: The curve of radially mapped points R_ε and its image $T^s_\varepsilon(R_\varepsilon)$.

Fig. 131 shows the curve R_ε formed by these points, and its image $T^s_\varepsilon(R_\varepsilon)$ which cuts R_ε in an even number of points because the area enclosed by R_ε and $T^s_\varepsilon(R_\varepsilon)$ must be the same.

The points common to R_ε and $T^s_\varepsilon(R_\varepsilon)$ are the fixed points of T^s_ε, and we can see in Fig. 132 that an alternating sequence of elliptic and hyperbolic fixed points emerges.

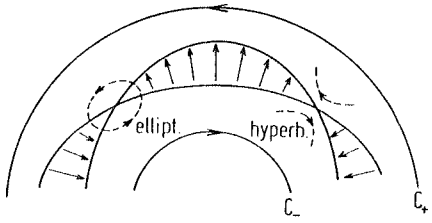

Fig. 132: Alternating hyperbolic and elliptic fixed points of T^s_ε.

This means that the original torus with rational frequency ratio is not completely destroyed under a perturbation, but there remains an even number of fixed points. This is the „Poincaré-Birkhoff theorem" (Birkhoff, 1935).

Let us first consider the elliptic fixed points which are surrounded by rotating points (see Figs. 125, 132). The corresponding orbits are the Poincaré sections of smaller tori for which all our arguments can be repeated; that is, some of these smaller

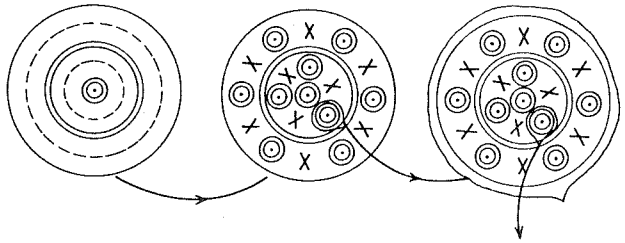

Fig. 133: Tori with rational frequency ratio decay into smaller and smaller tori, and the pattern of newly created elliptic and hyperbolic fixed points shows self-similarity.

tori are again stable according to the KAM theorem and other tori decompose into smaller ones according to the Poincaré-Birkhoff theorem. This gives rise to the self-similar structure in Fig. 133.

Homoclinic Points and Chaos

Which role do the hyperbolic fixed points play? Fig. 134 shows that, near a hyperbolic fixed point H, the motion becomes unstable, and orbits are driven away from it, in contrast to the stable rotational motion around an elliptic fixed point.

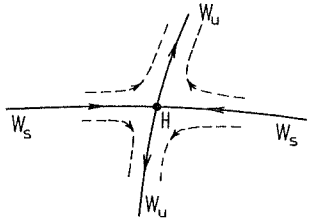

Fig. 134: Hyperbolic fixed point H with stable (W_s) and unstable (W_u) lines.

The stable (W_s) and unstable (W_u) lines which lead to or emanate from H behave highly irregularly since:

a) They cannot intersect themselves (otherwise the motion on a trajectory in phase space would not be unique for a given set of initial conditions),

b) but W_u can intersect W_s at a so-called homoclinic point (see Fig. 135).

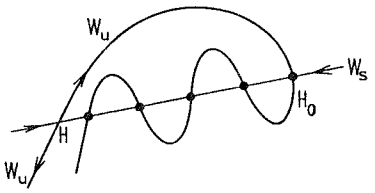

Fig. 135: Homoclinic points H_0 are the intersections of W_u and W_s.

Because the map T_ε^s is continuous, and a homoclinic point is no fixed point, repeated application of T_ε^s produces new homoclinic points. Furthermore, T_ε^s must be applied an infinite number of times to approach the hyperbolic fixed point H along W_s (Appendix G.) Between each homoclinic point H_0 and H there is, therefore, an infinite number of other homoclinic points; that is, the curves W_u and W_s form an extremely complex network.

Summarizing: If we disturb the regular orbits of an integrable system on a torus in phase space by adding a nonintegrable perturbation, then, depending on the different initial conditions (different $\vec{J}$, $\vec{\delta}$ in (6.7)) imply different ω_1/ω_2 since $\vec{\omega} = \vec{\omega}(\vec{J})$, regular or completely irregular motion results. Although the measure of initial conditions, which lead to regular motion, is nonzero due to the KAM theorem, for every rational frequency ratio (which are densely distributed along the real axis) one obtains smaller and smaller stable tori and irregular orbits due to the hyperbolic fixed points. Thus, an arbitrarily small change in the initial conditions leads to a completely different long-time behavior; and for the motion in phase space, one obtains the complicated pattern in Fig. 136. It shows that in conservative systems regular and irregular motion are densely interweaved.

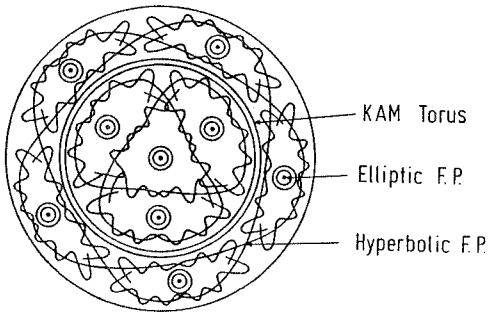

Fig. 136: Regular and irregular motion in the phase space of a nonintegrable system.

Finally, we also mention that for area-preserving maps one finds "period doubling", i. e. a successive creation of new pairs of *elliptic* fixed points (Greene et al., 1981). We shall discuss this scenario in Appendix G and show that the corresponding Feigenbaum constants are larger than in the dissipative case.

Arnold Diffusion

So far in this section we have only dealt with systems having two degress of freedom for which the two-dimensional tori stratify the three-dimensional energy surface S_E. The irregular orbits which traverse regions where rational tori have been destroyed are therefore trapped between irrational tori. They can only explore a region of the energy surface which, while three-dimensional, is nevertheless restricted and, in particular, disconnected from other irregular regions, as shown in Fig. 137.

For more degrees of freedom, however, the tori do not stratify S_E (e. g. for three degrees of freedom the tori are three-dimensional, and the energy surface is five-dimensional). The gaps then form one single connected region. This offers the possibility of so-called "*Arnold diffusion*" of irregular trajectories (Arnold, 1964). The existence of invariant tori for perturbed motion is, therefore, not a guarantee of stability of motion for systems with more than two degrees of freedom because irregular wandering orbits that are *not* trapped exist arbitrarily close to the tori.

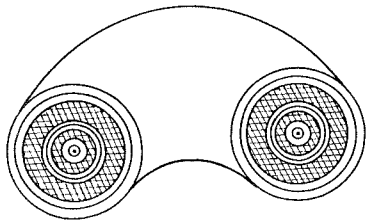

Fig. 137: Trapping of irregular orbits between stable KAM tori for a system with two degrees of freedom.

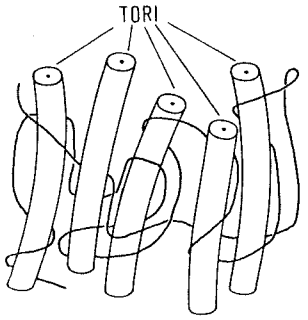

Fig. 138: Arnold diffusion for Hamiltonian systems with more than two degrees of freedom (schematically).

Finally, we present some experimental evidence for the coexistence of regular and irregular motion. Fig. 139 shows the Poincaré map in S for the nonintegrable Hénon-Heiles system,

$$H = \frac{1}{2} p_1^2 + q_1^2 + p_2^2 + q_2^2 + \left[q_1^2 q_2 - \frac{q_2^3}{3} \right] \tag{7.34}$$

which consists of an integrable pair of harmonic oscillators coupled by nonintegrable cubic terms (Hénon, Heiles, 1964). The left-hand column shows the surfaces of section generated by eighth-order perturbation theory for various energies (after Gustavson, 1966). The right-hand side are the computed intersections of the trajectory with S. For $E = 1/24$ and E 1/12, the mapping plane is covered with the intersections of (somewhat deformed) tori which signal regular motion and which are identical with those given by perturbation theory. Above $E = 1/9$, however, most, but not all, tori are destroyed, and all the dots which appear to be random are generated by one trajectory as it crosses S. The figure for $E = 1/8$ clearly shows the coexistence of regular and irregular motion.

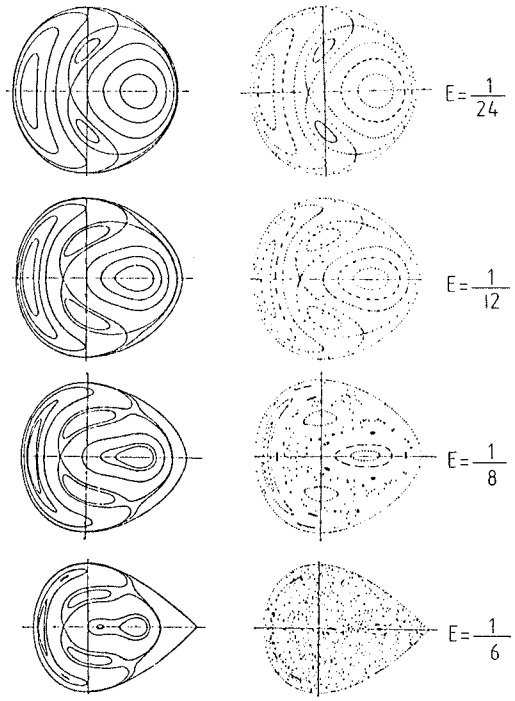

Fig. 139: Poincaré maps for the Hénon-Heiles system (after Berry, 1978).

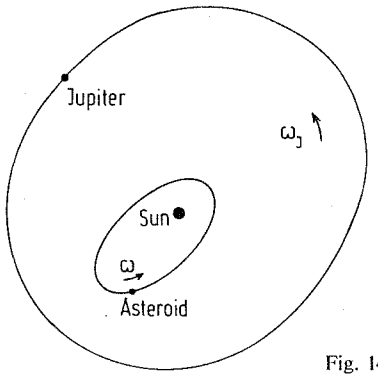

Fig. 140: Perturbation of an asteroid's motion by Jupiter.

As a further example, we consider the motion of an asteroid around the sun, perturbed by the motion of Jupiter, as shown in Fig. 140.

This three-body problem is nonintegrable, and according to eqns. (7.24–25) we expect that the asteroid motion becomes unstable if the ratio of the unperturbed frequency of the asteroid motion ω and the angular frequency of Jupiter ω_J becomes rational. Fig. 141 illustrates that, in fact, gaps occur in the asteroid distribution for rational ω/ω_J. On the other hand, the existence of stable asteroid orbits ($f \neq 0$) can be considered as a confirmation of the KAM theorem.

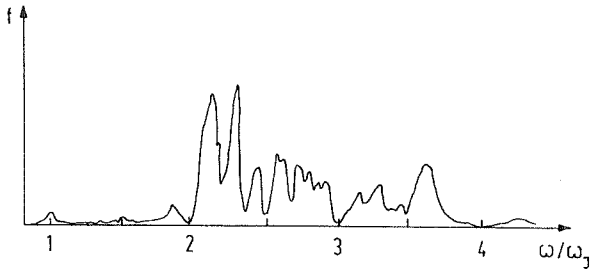

Fig. 141: Fraction f of asteroids in the belt between Mars and Jupiter as a function of ω/ω_J (after Berry, 1978).

A second sort of solar-system gaps occurs in the *rings of Saturn.* In this system Saturn is the attractor; the perturber is any of the inner satellites, and the rest masses are the ring particles. One major resonance occurs within the "Cassini division" shown on Plate VII at the beginning of the book.

7.2 Strongly Irregular Motion and Ergodicity

In the previous section, we linked the origin of irregular motion in Hamiltonian systems to hyperbolic fixed points in the associated area-preserving maps. If we, therefore, want to construct models for strongly irregular motion, it is natural to search for maps for which all fixed points are hyperbolic.

Cat Map

One example of such a system is Arnold's cat map on a torus which is defined by

$$\left.\begin{aligned} x_{n+1} &= x_n + y_n \bmod 1 \\ y_{n+1} &= x_n + 2y_n \bmod 1 \end{aligned}\right\} \equiv T\begin{pmatrix} x_n \\ y_n \end{pmatrix} \tag{7.35}$$

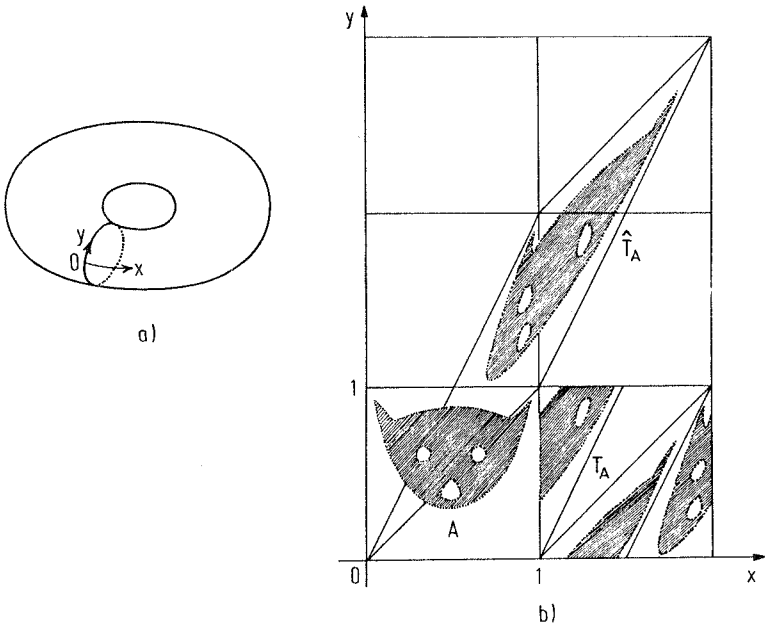

Fig. 142: Action of the map T on a cat on a torus. The torus a) is transposed into the unit square of b). $\hat{T}$ is the map T without restriction to the torus. (After Arnold and Avez, 1968.)

This map is area-preserving because the Jacobian of T is unity, and it has the eigenvalues

$$\lambda_1 = (3 + \sqrt{5})/2 > 1 \quad \text{and} \quad \lambda_2 = \lambda_1^{-1} < 1 \tag{7.36}$$

so that all fixed points of T^n ($n = 1, 2, 3 \ldots$) are hyperbolic. Any point on the torus for which x_0 and y_0 are rational fractions is a fixed point of T^n for some n (e.g. (0, 0) is a fixed point of T, and (2/5, 1/5) and (3/5, 4/5) are fixed points of T^2, etc.), and these are the only fixed points because T has integral coefficients.

The action of the cat map is illustrated in Fig. 142. After just one iteration the cat is wound around the torus in complicated filaments; its dissociation arises from the hyperbolic nature of T which causes initially close points to map far apart.

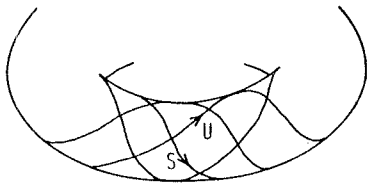

Fig. 143: Motion of W_u and W_s under the cat map.

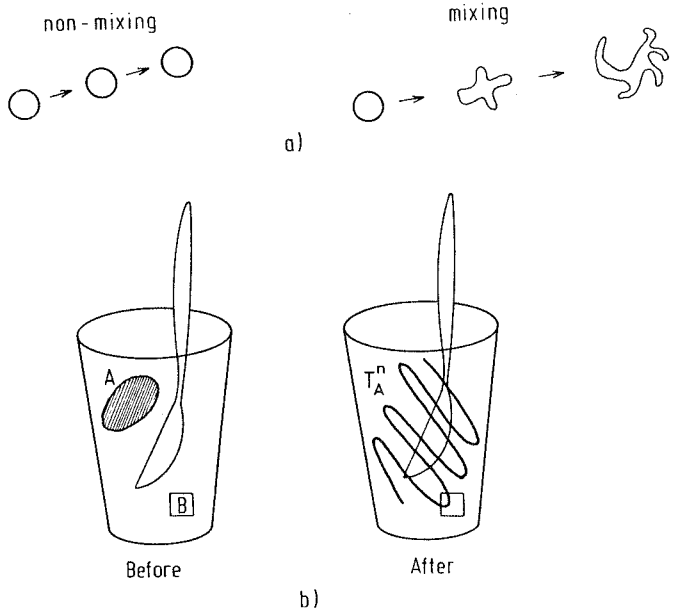

Fig. 144: a) Behavior of a volume element for nonmixing and for mixing transformations. b) Mixing of a drop of ink in a glass of water. (After Arnold and Avez, 1968.)